Nanoscale Electrochemical Movies and Synchronous Topographical Mapping of Electrocatalytic Materials

Cameron L. Bentley[*] *and Patrick R. Unwin*[*]

Department of Chemistry, University of Warwick, Coventry CV4 7AL, U.K.

[*]Email: C.Bentley.1@warwick.ac.uk (C.L.B.) and P.R.Unwin@warwick.ac.uk (P.R.U.)

Abstract. Techniques in the scanning electrochemical probe microscopy (SEPM) family have shown great promise for resolving nanoscale structure-function (*e.g.*, catalytic activity) at complex (electro)chemical interfaces, which is a long-term aspiration in (electro)materials science. In this work, we explore how a simple meniscus imaging probe, based on an easily-fabricated, single-channeled nanopipet (inner diameter ≈ 30 nm) can be deployed in the scanning electrochemical cell microscopy (SECCM) platform as a fast, versatile and robust method for the direct, synchronous electrochemical/topographical imaging of electrocatalytic materials at the nanoscale. Topographical and voltammetric data are acquired synchronously at a spatial resolution of 50 nm to construct maps that resolve particular surface features on the sub-10 nm scale and create electrochemical activity movies composed of hundreds of potential-resolved images on the minutes timescale. Using the hydrogen evolution reaction (HER) at molybdenite (MoS_2) as an exemplar system, the experimental parameters critical to achieving a robust scanning protocol (*e.g.*, approach voltage, reference potential calibration) with high resolution (*e.g.*, hopping distance) and optimal scan times (*e.g.*, voltammetric scan rate, approach rate etc.) are considered and discussed. Furthermore, sub-nanoentity reactivity mapping is demonstrated with glassy carbon (GC) supported single-crystalline {111}-oriented two-dimensional Au nanocrystals (AuNCs), which exhibit uniform catalytic activity at the single-entity and sub-single entity level. The approach outlined herein signposts a future in (electro)materials science in which the activity of electroactive nanomaterials can be viewed *directly* and related to structure through electrochemical movies, revealing active sites *unambiguously*.

1. Introduction

Technologically important electrochemical interfaces possess structural heterogeneity on length scales spanning several orders-of-magnitude (*i.e.*, sub-nm to mm) and even model interfaces (*e.g.*, single crystals) contain defects that may influence overall activity. In spite of this, there is an over-dependence in (electro)materials science on macroscopic "bulk" voltammetric techniques, which are not well-suited to analyzing the spatially heterogeneous (non-uniform) fluxes at complex electrochemical interfaces. Thus, techniques that can resolve nanoscale structure-activity at complex electrochemical interfaces and ensembles are recognized to be increasingly important.[1-6] Herein, we demonstrate how a simple meniscus imaging probe based on an easily-fabricated single-channeled nanopipet (diameter, $d \approx 30$ nm) can be used to carry out synchronous electrochemical/topographical imaging with high spatial resolution, to provide movies of electrocatalytic materials in action.

There is a limited set of techniques for nanoscale electrochemical flux mapping,[7-11] among which scanning electrochemical probe (SEPM) methods,[7, 8] most commonly scanning electrochemical microscopy (SECM),[12-14] are attracting significant interest. A major limitation of SECM is that it offers no inherent positional feedback when operated in the most common constant plane scanning mode, meaning that the response of the tip is convoluted by the reactivity and topography of the substrate (electrode) surface.[8] Moreover, positioning and scanning a tip a few to tens of nm above a surface, without positional feedback, limits the types of substrates that can be studied and this scanning mode becomes increasingly challenging to implement practically. Although the topography-activity conundrum inherent in SECM can be overcome through the use of dual redox mediators (*i.e.*, one to indicate on topography and the other to measure reactivity)[15] or the integration of SECM with other scanning probe techniques such as atomic force microscopy (AFM)[16, 17] or scanning ion conductance microscopy (SICM)[18, 19], fabricating reproducible nanoelectrode probes is non-trivial and time-consuming,

which is further complicated when multi-channel probes are to be employed.[8] To circumvent this issue, recent studies have shown how an easily-fabricated nanopipet probe can be deployed in a multifunctional SICM format to perform synchronous topographical imaging and electrochemical flux mapping at the nanoscale.[20, 21]

It is important to point out that when performing reaction mapping with SECM or SICM, activity is measured *indirectly* by monitoring the spatially-dependent fluxes of reactant, product or intermediates at the tip.[8, 12-14, 20, 21] For this reason, these methods suffer from diffusional broadening, where neighbouring sites on a surface may interact (*i.e.*, diffusional cross-talk), making "single-entity" activity mapping within an ensemble of active materials very challenging. Furthermore, the need to immerse the entire surface for the duration of an experiment (typically up to tens of minutes for a single image frame) complicates sample preparation and renders the technique susceptible to surface aging effects induced by electrolyte exposure (*e.g.*, in corrosion measurements) or turnover at the surface of interest (*e.g.*, in catalytic activity measurements). In SECM, care must also be taken to ensure the tip activity is robust, which is non-trivial, given the high rates of mass transport to nanoscale electrodes.[22, 23]

By contrast, in droplet cell-based SEPM techniques such as scanning electrochemical cell microscopy (SECCM), the electrochemical properties of a surface are probed *directly* and *locally* with integrated probe positional feedback.[24, 25] In SECCM, electrochemical measurements are performed within a confined area of a surface, defined by the dimensions of a droplet (meniscus) formed at the end of a pulled glass capillary, with probe (tip) diameters typically in the hundreds of nm[26-29] to μm[30, 31] range. SECCM has mainly been operated in the constant-distance, constant potential scanning mode,[30, 31] which provides an electrochemical map and topography simultaneously, however recent studies have shown the strength of the voltammetric "hopping" mode,[29, 32-34] where spatially-resolved electrochemical flux movies

comprising hundreds of frames over large potential ranges (> 1 V) can be constructed. Through combination with complementary imaging and spectroscopic techniques, applied to the same areas of the electrochemically mapped sample, in a *correlative multi-microscopy approach*, SECCM has previously been utilized to elucidate structure-function in many classes of nanomaterial, including sp^2 carbon materials (*e.g.*, graphene, nanotubes and highly-ordered pyrolytic graphite),[27, 35, 36] catalytic nanoparticles (NPs)[37, 38] and a range of hydrogen evolution catalysts (*e.g.*, MoS_2 and $Fe_{4.5}Ni_{4.5}S_8$)[29, 34].

In a recent study,[39] we demonstrated how voltammetric hopping mode SECCM with fine, single-channeled nanopipets (diameter, $d \approx 30$ nm) could be used to carry out synchronous electrochemical/topographical imaging at complex electrocatalytic interfaces with high spatiotemporal resolution. We utilized this methodology to perform sub-nanoentity (*i.e.*, sub-NP) electrochemical imaging for the first time with an SEPM technique, a feat which had previously been limited to super-high-resolution optical imaging.[9-11] We build upon that work here by revisiting the hydrogen evolution reaction (HER)/MoS_2 system in order to provide an expanded discussion on the operational principles of the technique. We also further demonstrate the general applicability of this methodology by applying it to perform sub-particle (*i.e.*, sub-single entity) topographical and electrochemical flux mapping on glassy carbon (GC)-supported two-dimensional (2D) Au nanocrystals (AuNCs).

2. Experimental

Chemical Reagents and Electrode Materials. Perchloric acid ($HClO_4$, Sigma-Aldrich, 70%), sulfuric acid (H_2SO_4, Sigma-Aldrich, 96%) and chloroauric acid ($HAuCl_4.xH_2O$, Sigma-Aldrich, 99.995%) were used as supplied by the manufacturer. All solutions were prepared with deionized water (resistivity = 18.2 MΩ.cm at 25°C, Integra HP, Purite, U.K.).

The naturally-occurring molybdenite (MoS_2) crystal, previously shown to be the semiconducting 2H phase,[34] was purchased from Manchester Nanomaterials Ltd (U.K.). Prior to use, MoS_2 flakes were fixed in place on a glass microscope slide using copper scanning electron microscopy (SEM) tape and mechanically cleaved using the "scotch-tape method".[40] In order to avoid possible issues arising from ohmic resistance, the freshly-cleaved MoS_2 flakes were electrically connected through top-contact with the conductive copper SEM tape. The glassy carbon (GC) substrate, purchased from HTW-Germany, was polished roughly with an aqueous slurry of 0.05 μm Al_2O_3 (Buehler, U.S.A.) prior to use.

The 2D Au nanocrystals were prepared by reducing $AuCl_4^-$ (from $HAuCl_4$) with lemongrass extract, as per a literature procedure.[11, 41] Briefly, 50 g lemongrass (*Cymbopogon flexuosus*) was finely cut and boiled in 250 mL of deionized water for 5 minutes. The lemongrass suspension (broth) was subsequently cooled to room temperature and then 5 mL of it was added to 45 mL of 1 mM $HAuCl_4$ solution. The reaction solution was then cooled, incubated overnight at room temperature and purified by three cycles of centrifugation at 3000g, before being resuspended in 50 mL of deionized water. The AuNC ensemble was prepared by drop-casting the resuspended solution onto GC, which was subsequently washed by ultrasonication in deionized water and then dried under a stream of nitrogen. Prior to use, the AuNC/GC ensemble was electrically connected, and conditioned by cycling voltammetrically between *ca.* +0.1 and -0.5 V *vs.* the reversible hydrogen electrode (RHE) at 0.5 V s^{-1} for 10 cycles in an O-ring cell format.[42] Field-emission SEM images of the AuNC

ensemble were obtained with a GeminiSEM 500 scanning electron microscope (Zeiss, Germany), at an acceleration voltage of 10 kV, with an SE2 detector.

The palladium-hydrogen (Pd-H_2) quasi-reference counter electrode (QRCE) was prepared by biasing a Pd wire (0.25 mm diameter, Goodfellow, 99.95%) at −3 V *vs.* a Pt counter electrode in a 0.1 M $HClO_4$ solution. The QRCE potential was calibrated against a commercial saturated calomel electrode (SCE) immediately after each experiment, which has a potential of +0.241 V *vs.* the standard hydrogen electrode (SHE).

Electrochemical Measurements. Preconditioning was performed in a three-electrode format with a Pd-H_2 QRCE and platinum wire (Goodfellow, U.K.) auxiliary electrode on a FAS2 Femtostat (Gamry Instruments, U.S.A.). All other electrochemical experiments were carried out in the SECCM format on a home-built electrochemical workstation.[25, 43] In this configuration (shown schematically below in Figure 1), a single-barreled nanopipet probe was filled with electrolyte solution (detailed below) and mounted on a *z*-piezoelectric positioner (P-753.1CD or P-753.3CD, Physik Instrumente, Germany). The opening of the nanopipet probes was circular, with an internal diameter of *ca.* 30 nm. A Pd-H_2 wire placed in the nanopipet barrel, through the back, served as a QRCE. The nanopipet probe was positioned above the substrate surface using stepper motors (8303 Picomotor Actuator, Newport, U.S.A.) for coarse movement and an *xy*-piezoelectric positioner (P-622.2CD or P-733.2DD, Physik Instrumente, Germany) for fine movement. During each approach, surface current (i_{surf}) was used as feedback to detect when the meniscus cell had made contact with the substrate (working electrode) surface. The magnitude of the threshold current herein was *ca.* 1.5 pA. The nanopipet itself never made contact with the substrate. Voltammetric measurements were performed in the confined area defined by the meniscus cell created between the probe tip and substrate surface.

Electrochemical measurements at the substrate (working electrode) were made using a linear-sweep voltammetric "hopping" regime, as previously reported.[27, 32, 33, 39] In brief, the nanopipet probe was approached to the substrate surface at a series of predefined locations in a grid and, upon each landing, an independent LSV measurement was made, building-up a voltammetric 'image' of the substrate. The final position of the *z*-piezoelectric positioner at approach (*i.e.*, *z*-extension) was also used to build up a topographical map of the substrate synchronously. The hopping distance (*i.e.*, *x*-*y* spatial resolution) was 50 nm.

The SECCM set up was situated in an aluminum Faraday cage equipped with heat sinks and vacuum panels to minimize noise and thermal drift. The Faraday cage was installed on an optical table (RS2000, Newport, U.S.A.) with automatic levelling isolators (Newport, S-2000A-423.5). The QRCE potential was controlled, with respect to ground and the current flowing at the substrate (working electrode), held at a common ground, was measured using a home-built electrometer. The current was measured every 4 µs, which was averaged 65 times to give a data acquisition rate of 260 µs (*i.e.*, 1 data point ever 2.6 mV at 10 V s^{-1}). A home-built 8th order (low-pass) brick-wall filter unit with a time constant of 200 µs was utilized during data (current) acquisition. Data acquisition and instrumental control was carried out using an FPGA card (PCIe-7852R) controlled by a LabVIEW 2016 (National Instruments, U.S.A.) interface running the Warwick Electrochemical Scanning Probe Microscopy (WEC-SPM, *www.warwick.ac.uk/electrochemistry*) software.

The single-barreled nanopipet probes were fabricated from quartz filamented capillaries (QTF120-90-100, Friedrich & Dimmock Inc., U.S.A.) using a CO_2-laser puller (P-2000, Sutter Instruments, U.S.A.; pulling parameters: Line 1: HEAT 750, FIL 4, VEL 30, DEL 150, PUL 80; Line 2: HEAT 650, FIL 3, VEL 40, DEL 135, PUL 150). Representative nanopipet tips were imaged using transmission electron microscopy (TEM) on a Jeol 2100 Transmission Electron Microscope (Jeol, Japan) operating at an acceleration voltage of 200

kV. After the nanopipet probes were filled with the analyte solution using a MicroFil syringe (World Precision Instruments Inc., U.S.A.), a thin layer of silicone oil (DC 200, Sigma-Aldrich) was added on top in order to minimize evaporation. The QRCE was then inserted through the silicone layer, into the analyte solution, and mounted on the *z*-piezoelectric positioner, as described above.

After acquisition, the raw data were processed using the Matlab R2015b (8.6.0.267246, Mathworks, U.S.A.) software package. Sample tilt/*z*-piezoelectric positioner drift was corrected using the scanning probe image processing software package (SPIP v. 6.0.14, Image Metrology, Denmark). Data plotting was carried out using the Matlab R2015b and OriginPro 2016 64bit (b9.3.226, OriginLab, U.S.A.) software packages. All topographical and electrochemical activity maps (and movies) were plotted in Matlab, with no data interpolation.

3. Results and Discussion

Operational principles. In most SECCM studies, a dual-channel pipet (hundreds of nm[26-29] to µm[30, 31] in diameter) is employed and the feedback signal used to position the probe relative to surface of interest is an ion conductance current (i_{ion}), induced by applying a bias between QRCEs placed in the barrels of the probe. During operation, the probe is mechanically oscillated in the *z*-direction to induce *ac* modulation in i_{ion}, termed i_{ac}, which is very sensitive to the morphology of the meniscus formed at the end of the pipet and can therefore be used as a feedback signal to make meniscus contact with (semi)conducting and insulating surfaces.[24, 25, 43] Although i_{ac} feedback control is very robust, physical modulation of probe limits the *z*-approach rate achievable in SEPM techniques, making *dc* feedback modes advantageous for high-speed imaging.[7, 44] One option is to use the *dc* component of i_{ion}, termed i_{dc}, which, although susceptible to drift, has been shown to be a viable feedback type in SICM when operated in a self-referencing regime.[45] The second option, which has been employed herein, is to employ surface current (i_{surf}) feedback[26, 46] with a single-channel nanopipet probe. In addition to being much faster than "dual-channel" SECCM, the instrumental set up is also greatly simplified using this approach, only requiring *x*-*y*-*z* piezoelectric positioners, a current follower (electrometer), a wave-form generator (digital herein) and a data acquisition system (FPGA card, detailed in the Experimental Section).

The instrumentation and working principles of the SECCM setup used herein are shown schematically in Figure 1a. SECCM has been operated in the voltammetric "hopping" mode regime,[32-34] where the nanopipet probe is approached to the surface of interest at a series of predefined locations in a grid and, upon each landing, a voltammetric (linear-sweep, cyclic or potential-step waveforms) experiment is carried out to build up an electrochemical 'map' of the substrate (see Figure 1a). The *z*-position, applied potential (E_{app}) and i_{surf} (as a function of time), recorded synchronously during a single "hop" of a scanning experiment on a AuNC

substrate (supported on GC, explored further below) is shown in Figure 1b. During the initial approach [Figure 1b, **(1)**], E_{app} was chosen to be sufficient to drive the reaction of interest (*e.g.*, HER herein) at the substrate upon landing, in order to generate a reliable feedback signal (i_{surf}) for positional control. When the meniscus protruding from the end of the nanopipet probe (schematic representation in Figure 1a) initially made contact with the substrate surface (note, the probe itself did not make contact), a two electrode electrochemical cell was formed and a reductive transient in i_{surf} resulted as the reaction of interest (*e.g.*, HER) was driven at the working electrode (*e.g.*, AuNC surface) within the confined area of the meniscus cell. Upon detecting a preset threshold ("feedback") current ($i_{surf} \approx -1.5$ pA herein), the *z*-approach was immediately stopped and E_{app} was switched to the initial potential, resulting in an oxidative transient in i_{surf}, attributable to double-layer charging current [Figure 1b, **(2)**]. After a pre-defined hold-time (0.005 s in Figure 1b), the E_{app}-*t* waveform (linear sweep at a scan rate, *v*, of 10 V s^{-1} in Figure 1b) was applied and i_{surf} was recorded concurrently [Figure 1b, **(3)**], to give rise to a spatially resolved linear-sweep voltammogram (LSV). After holding at the final potential [Figure 1b, **(4)**] for a pre-defined hold time (0.001 s in Figure 1b), the probe was retracted and E_{app} was switched back to the initial approach value for the next hop [Figure 1b, **(5)**].

The procedure outlined above was repeated at each and every hop (pixel) of the scan and i_{surf} at a given E_{app} was plotted against *x*–*y* position to produce electrochemical (voltammetric) "maps" of the substrate. The individual i_{surf}–E_{app} "frames" were then combined to produce electrochemical movies, which consider the spatially-resolved activity of the surface (*e.g.*, AuNCs on GC) over a large potential range (*i.e.*, a range of current densities, *J*). In addition, the final *z*-position of the piezoelectric positioner during approach [Figure 1b-i, **(3)**] is also plotted against *x*-*y* position to produce a high-resolution topographical image of the substrate. Although in the case of AuNCs/GC and MoS_2 (explored below), correlation between

the topographical and electrochemical maps reveals the active site (*vide infra*) *unambiguously*, the scanned area is amenable to further analysis by other high resolution microscopy/spectroscopy to resolve nanoscale structure-activity directly.[29, 34, 36]

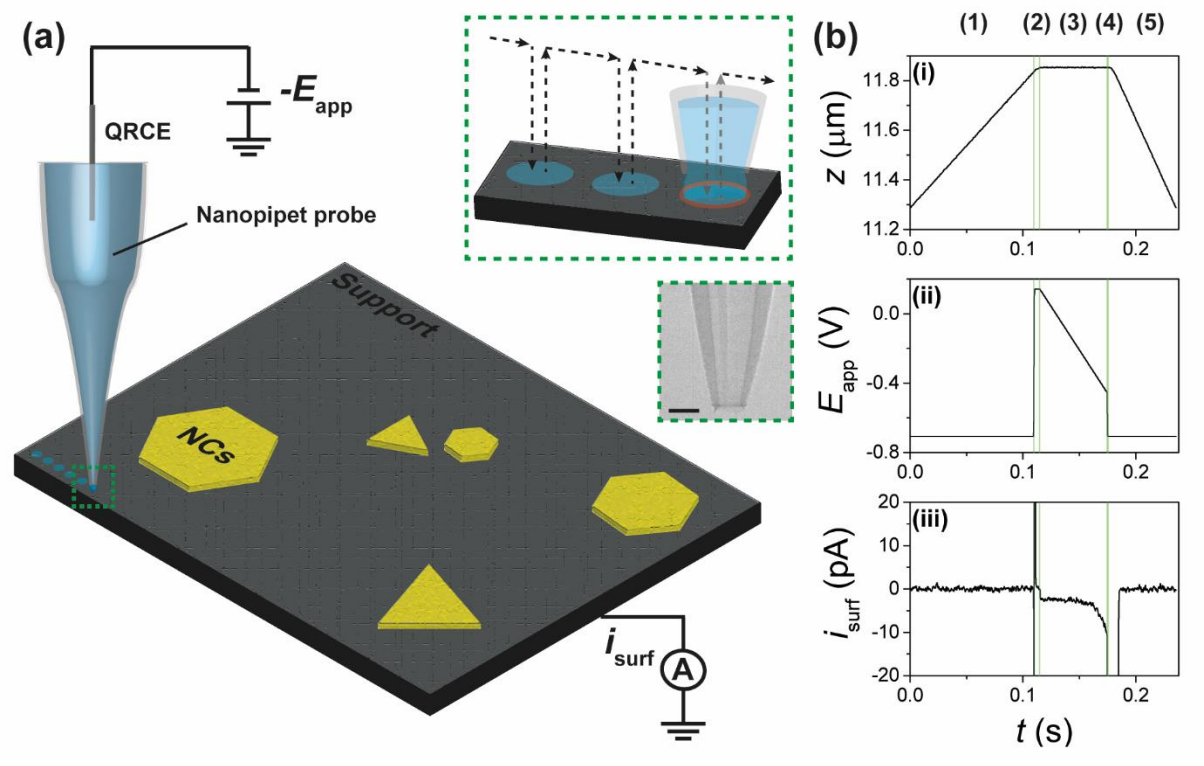

Figure 1. (a) Schematic showing nanoscale synchronous electrochemical/topographical mapping using voltammetric hopping mode SECCM with a single-channel nanopipet probe (TEM image of the end of a representative nanopipet probe is shown inset, scale bar indicates 40 nm). In this configuration, a voltage was applied directly at the QRCE to control the working electrode potential (E_{app}), and the working electrode current (surface current, i_{surf}) was measured. i_{surf} also serves as the feedback signal to detect meniscus-surface contact during approach. Arrows indicate movement of the nanopipet probe along the surface during scanning (inset, top-right). **(b)** Plots of **(i)** *z*-extension, **(ii)** E_{app} and **(iii)** i_{surf} during a "single hop" at a AuNC substrate (supported on GC, see below) with a nanopipet probe containing 100 mM H_2SO_4. Experimental parameters are as follows: voltammetric scan rate (ν) = 10 V s^{-1} and data acquisition time (t_d) = 260 µs.

Methodology and applications: HER at MoS_2. Herein, the methodology described above, combined with the use of a fine, single channeled nanopipet probe ($d \approx 30$ nm, TEM image shown inset in Figure 1a) has enabled fast, high-resolution synchronous topography/activity mapping of electrocatalytic materials at the nanoscale. The nanopipet probes were reproducibly fabricated with a laser pipet puller, using the pulling parameters outlined in the Experimental Section. Examples of high-quality topographical and electrochemical images produced using this methodology are shown in Figure 2, obtained from MoS_2, a promising earth-abundant HER electrocatalyst.[47, 48] A thorough analysis of this material has already been carried out in two recent SECCM studies,[34, 39] where it was shown unequivocally that the HER is greatly facilitated at the edge plane (EP) relative to the basal plane (BP), with up to *ca.* 30-fold higher current densities (*J*) measured at surface defect sites (*e.g.*, multiple-layer step edges). For this reason, such an analysis will not be carried out here, rather the experimental parameters critical to a robust scanning protocol (*e.g.*, approach voltage, reference potential calibration) with high spatial resolution (*e.g.*, hopping distance) and optimal scan times (*e.g.*, voltammetric scan rate, approach rate etc.) will be considered and discussed. In other words, this section is intended to serve as a "practical guide" to those interested in utilizing SECCM for nanoscale electrocatalytic imaging.

From Figure 2a, it is clear that the 2.5×2.5 μm scan area is predominantly BP, with two surface "features" (defects): a *ca.* 10 nm deep crevice and a *ca.* 40 nm high step (line scan profile shown in Figure 2c). Comparing Figure 2a and b, it can be concluded that the BP possesses uniform activity on the micrometer (μm) length scale (*i.e.*, i_{surf} is uniform at the BP) and that the HER kinetics are greatly accelerated at the EP (exposed at the surface defect sites, see correlation between *z*-position and i_{surf} line scan profiles in Figure 2c). As alluded to above, an LSV experiment was carried out at each pixel, allowing the spatially-resolved i_{surf}–E_{app} data to be presented as an electrochemical flux movie (shown in the Supporting Information, Movie

S1). Alternatively, individual LSVs can be extracted and compared, as shown in Figure 2d, where it is evident that the enhancement in i_{surf} approximately scales with the geometry of the surface defect, as previously described.[34, 39] It should be noted that distortion of the meniscus cell is expected to be negligible at these surface defect sites (*e.g.*, multi-layer step edge and crevice), as explored in our previous work.[34, 39]

In Figure 2a and b, the lateral (*x*–*y*) resolution of the images (determined by the hopping distance, 50 nm) is limited by the dimensions of the nanopipet probe ($d \approx 30$ nm). 50 nm is the highest lateral resolution achieved with SECCM to date, achieved here and in our previous study,[39] but there is scope to further improve this, with laser pulled nanopipets of sub-10 nm diameter being reported elsewhere,[49] but not yet used for any kind of imaging. The spatially-resolved LSV-SECCM shown in Movie S1 is made up of 384 image frames (*i.e.*, 1 image every 2.6 mV), with each frame comprised of 2500 pixels, at a density of 400 pixels μm^{-2}. The map took *ca.* 635 seconds to complete, corresponding to pixel (resolved in space) and frame (resolved in E_{app}) acquisition rates of *ca.* 0.25 s per pixel and 1.65 s per frame, respectively. For each pixel, *x*–*y* movement, approach, LSV and retract took 0.017 s (0.05 µm at 3 µm s^{-1}), 0.08 s (0.4 µm at 5 µm s^{-1}), 0.115 s (1 V at 10 V s^{-1} + 0.01 s pre-LSV + 0.005 s post-LSV) and 0.04 s (0.4 µm at 10 µm s^{-1}), respectively. This is by far the fastest scan-speed reported with the voltammetric hopping mode regime and has a comparable frame-rate to the "high-speed" constant-potential, constant-distance SECCM approach previously reported by our group.[38] Nevertheless, there is further scope to improve this through the application of higher piezo translation rates (approach rates of up to 500 µm s^{-1} reported for SICM topographical imaging[50]) or shorter/faster *E*–*t* waveforms.

In Figure 2, an approach voltage (E_a) of –0.947 V was used, which is sufficient to drive the HER on both the EP and BP, ensuring a sizeable current transient during initial meniscus contact [Figure 1b, **(2)**], well above the feedback threshold (*ca.* −1.5 pA herein). This was

found to be very important for robust and reproducible electrochemical imaging, as less negative E_a values (*i.e.*, lower HER driving forces) resulted in occasional probe contact with the substrate surface during scanning over the BP (*i.e.*, tip crashing).

The relative humidity in the United Kingdom is relatively constant year-round (*ca.* 60 to 80%), and thus additional humidity control was not employed herein. Should humidity control be required (*i.e.*, due to tip-blockage caused by crystal formation), the substrate (working electrode) can be mounted in a humidified cell, as previously reported by our group and others.[28, 43, 51] Finally, the QRCE, Pd-H_2, is non-fouling and was found to possess a stable potential on at least the hours timescale (maximum tested and more than sufficient to acquire vast datasets as outlined here), particularly when placed in an enclosed volume of acidic solution (*i.e.*, within the nanopipet probe). Thus, calibration was performed immediately following a scan by placing the entire nanopipet probe (the end of the probe was broken to µm-scale to minimize tip resistance) in a bath of the analyte solution (*i.e.*, 0.1 M $HClO_4$ above) and calibrating potentiometrically against an SCE. This ensured that the calibrated electrochemical data were reliable and reproducible, confirmed by performing measurements on multiple samples of MoS_2 over a period of several weeks.

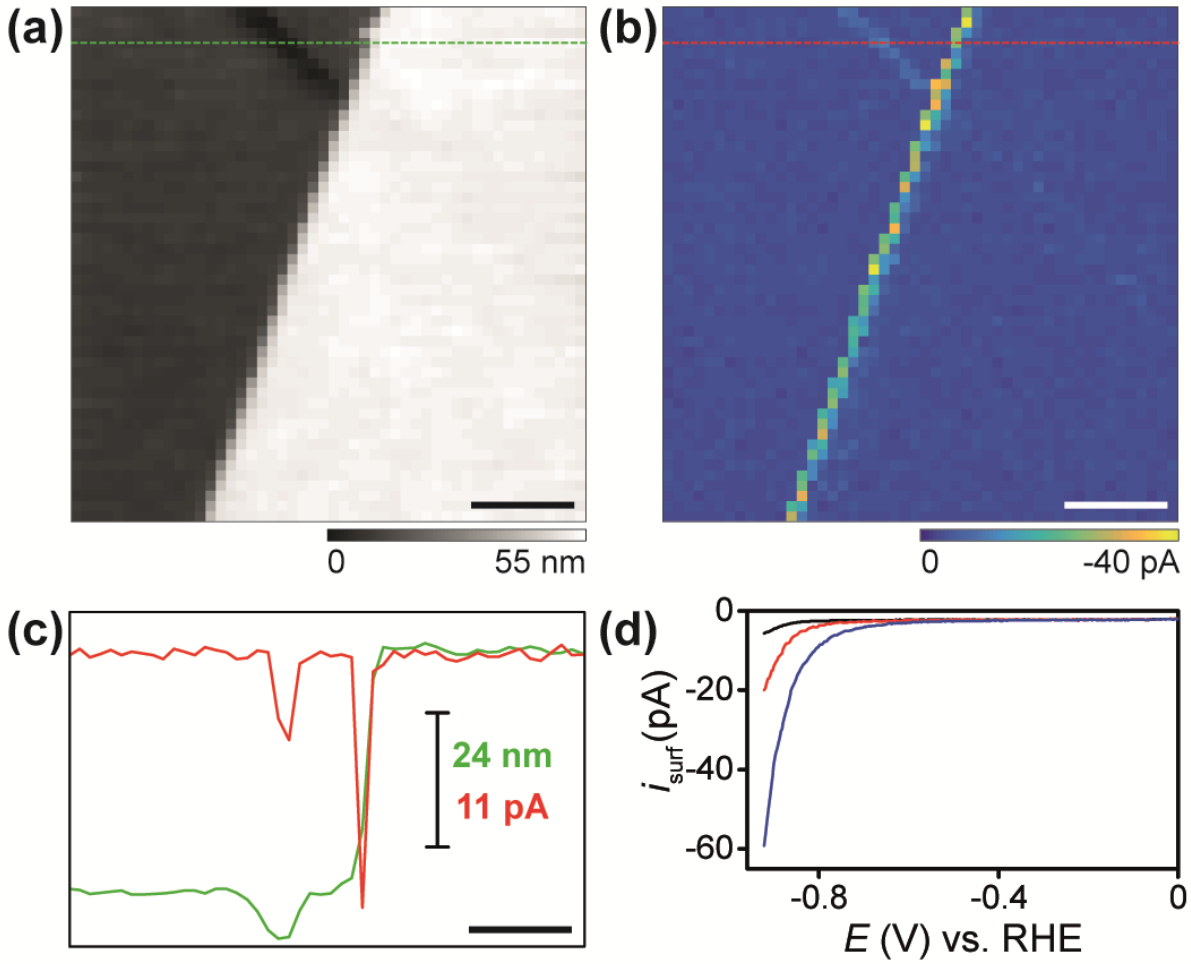

Figure 2. (a) Topographical and **(b)** spatially-resolved electrochemical maps (2500 pixels over a 2.5×2.5 µm scan area, 400 pixels µm^{-2}) obtained with the voltammetric hopping mode SECCM configuration (Figure 1), visualizing HER activity on bulk MoS_2. The nanopipet probe ($d \approx 30$ nm) contained 100 mM $HClO_4$. The electrochemical map was obtained at –0.87 V vs. RHE (see Movie S1 for the full potential range). **(c)** *z*-position and i_{surf} line scan profiles of the area indicated by the green and red dashed lines in **(a)** and **(b)**, respectively. 0 nm and 0 pA are the bottom-left and top-left corners of the plot, respectively. **(d)** Average LSVs obtained on the basal plane (black trace), crevice-defect (red trace) and step-defect (blue trace). Experimental parameters are as follows: $v = 10$ V s^{-1}, $t_d = 260$ µs, $t_s = 635$ s (*ca.* 0.25 s per pixel), $E_a = –0.947$ V, $E_i = 0.053$ V and $E_f = –0.947$ V (all vs. RHE). All *xy* scale bars indicate 500 nm. The data presented in **(a)** and **(b)** are not interpolated.

Probing the (electro)catalytic activity of 2D Au nanocrystals. Real (electro)catalysts are typically nanostructured, which serves to maximize the surface area of the active material and expose particular surface "active" sites (*e.g.*, defects). Metal NPs, which have found application in many fields spanning the physical and life sciences, including catalysis, have been shown in bulk ensemble studies to possess strongly size, shape and structure-sensitive (electro)catalytic activity.[2, 52, 53] Herein, 2D AuNCs, prepared by wet synthesis,[41] were dropcast onto a glassy carbon (GC) support to simulate a complex (electro)catalytic interface; representative SEM images are shown in Figure 3a. These single-crystalline {111}-oriented AuNCs are triangular (Figure 3a-i) or hexagonal (Figure 3a-ii) in shape and range in size from *ca.* 100 nm to > 1 μm, as shown in the Supporting Information, Figure S1. Note that the contrast or "patterning" visible on the surface of the AuNCs (Figure 3a) is commonly observed with thin Au nanoplates and has been attributed to bending or "buckling".[41, 54, 55]

The catalytic properties of these AuNCs was probed by cathodic polarization in an acidic solution (0.1 M H_2SO_4). As environmental control[31, 32] was not implemented, in this configuration there is an enhanced flux of O_2 due to the presence of an air-water-electrode three phase boundary[31] and thus the contribution from both the oxygen reduction reaction (ORR) and HER is expected to be significant in the investigated potential range (*vide infra*). Significant overlap between these two electrocatalytic processes is expected, as Au is known to be a poor electrocatalyst for the ORR in acidic media.[3] An E_a of −0.708 V was implemented to generate a reliable i_{surf} feedback signal on both the AuNC and GC surfaces. This negative potential pulse is also thought to have an *in situ* cleaning effect[31, 34], ensuring an active catalytic AuNC surface, prior to recording the LSV.

A topographical image of the AuNC/GC substrate, constructed from the spatially resolved *z*-positional data is shown in Figure 3b. There are four *ca.* 500 nm AuNCs in the 3.5 × 1.8 μm scan area, which are triangular (*e.g.*, AuNC-1) or hexagonal (*e.g.*, AuNC-3) in shape.

The AuNCs are flat (*i.e.*, 2D platelets) and *ca.* 12 nm in height, evident from the *z*-height line profile in Figure 3c. Also evident in the topographical image (Figure 3b) are scratches and wells in the GC support surface (arising during electrode polishing, confirmed by scanning an area of the surface where AuNCs are absent, as shown in the Supporting Information, Figure S2). The morphology of the probed AuNCs is in accordance with the original synthesis by Shankar et al.[41], who reported 2D triangular or hexagonal crystals with sizes and heights in the 0.05 to 1.8 μm and 8 to 18 nm range, respectively, determined by a combination of TEM and AFM. This is a testament to the high-quality of the topographical images achievable with the voltammetric hopping mode SECCM set up presented herein (see Figure 1).

A spatially-resolved LSV-SECCM movie of the scan area is shown in the Supporting Information, Movie S2. The movie consists of 230 image frames (*i.e.*, 1 image every 2.6 mV) and each pixel (70×36 = 2520 in total) represents an individual LSV in the 3.5×1.8 μm scan area (pixel density = 400 μm^{-2}). The map took *ca.* 671 seconds to complete, corresponding to pixel and frame acquisition rates of *ca.* 0.27 s per pixel and 2.92 s per frame, respectively. Individual frames from the movie, obtained at increasingly negative E_{app} are shown in Figure 4a to d. Through comparison of the electrochemical activity maps with the topographical map in Figure 3b, it is clear that the ORR/HER only occurs at the surface of the AuNCs in the investigated potential range (0.142 to –0.458 V *vs.* RHE), while the carbon support remains homogeneously inactive. It should be noted that there is no correlation between the topography (*z*-height) and measured current (i_{surf}) on the GC support surface (compare Figures 2b and 3a-d or Supporting Information, Figure S2a and b), indicating that morphology of the meniscus cell is very stable, in agreement with previous studies.[34, 39] This is further supported by the fact that the electrochemical and topographical "footprints" of the AuNCs are comparable, evident from the i_{surf} and *z*-height line scan profiles in Figures 2c and 3e (direct comparison in the Supporting Information, Figure S3).

Each of the AuNCs in the scan area (see Figure 3d) possess comparable activity (*i.e.*, at the single entity level), evident from the i_{surf} distribution in Figure 4f (or average LSVs, shown in the Supporting Information, Figure S4). From Figure 4f, it is also clear that each of the AuNCs is uniformly active (*i.e.*, at the sub-single entity level), with mean (± one standard deviation) i_{surf} @ –0.43 V vs. RHE values of –11 ± 2, –12 ± 2, –12 ± 2 and –11 ± 2 pA at AuNCs 1 to 4, respectively. This is not surprising, as the AuNCs are single-crystalline ({111}-oriented[41]) and are therefore expected to possess uniform activity for grain-orientation dependent electrocatalytic process such as the ORR or HER.[3] This contrasts directly with our previous study on hydrazine electro-oxidation at electro-deposited non-faceted AuNPs, where up to 5-fold differences in i_{surf} were measured at the sub-particle level.[39] Finally, it should be noted that slightly elevated i_{surf} is observed at the contact region between AuNC-1 and AuNC-2, as shown in Figure 4d. This may be attributable to enhanced catalytic activity [*i.e.*, due to exposure of the {110}-oriented edge[55]] or may arise from an increased surface area or enhanced O_2 flux across the air-meniscus interface,[31] in the particle contact region. Further work is underway to investigate the origin of this enhancement.

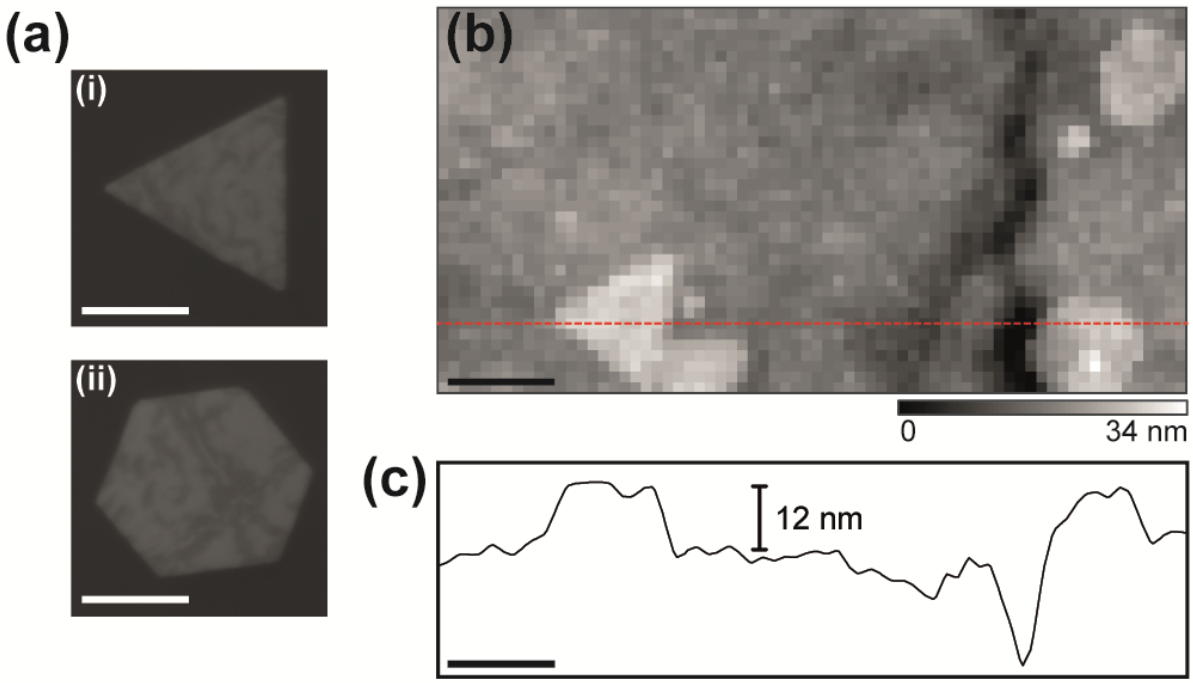

Figure 3. (a) Representative SEM images of a **(i)** triangular and **(ii)** hexagonal AuNC, supported on GC. **(b)** Topographical map (2520 pixels over a 3.5×1.8 µm scan area, 400 pixels μm^{-2}), constructed from the *z*-extension data collected during an SECCM experiment (configuration shown in Figure 1), visualizing ORR/HER activity on GC-supported AuNCs (*vide infra*). The nanopipet probe ($d \approx 30$ nm) contained 100 mM H_2SO_4. **(c)** *z*-position line scan profile of the horizontal region indicated by the red line in **(b)**. 0 nm is bottom-left corner of the plot. All *xy* scale bars indicate 500 nm. The data presented in **(b)** are not interpolated.

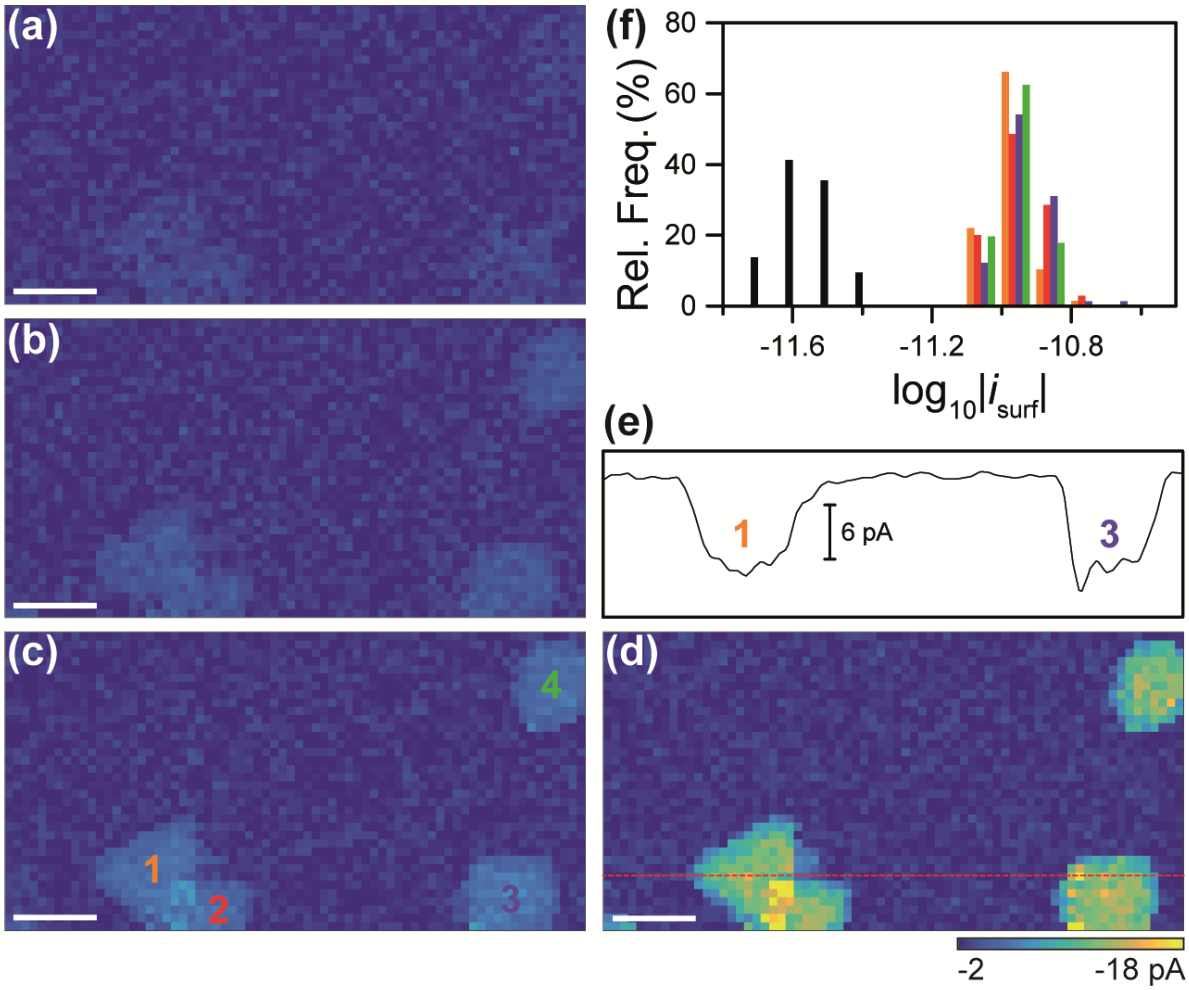

Figure 4. (a-d) Spatially-resolved electrochemical maps (2520 pixels over a 3.5×1.8 µm scan area, 400 pixels µm^{-2}) obtained with the voltammetric hopping mode SECCM configuration (Figure 1), visualizing ORR/HER activity on GC-supported AuNCs. The nanopipet probe ($d \approx$ 30 nm) contained 100 mM H_2SO_4. The electrochemical maps were obtained at **(a)** –0.16, **(b)** –0.25, **(c)** –0.34 and **(d)** –0.43 V vs. RHE (see Movie S2 for the full potential range). The AuNCs are labelled 1 to 4 in **(c)**. **(e)** i_{surf} line scan profile of the horizontal region indicated by the red line in **(d)**. 0 pA is top-left corner of the plot. **(f)** Normalized histogram showing the distribution in the logarithm of i_{surf}, arising from the ORR/HER at an applied potential of –0.43 V vs. RHE. GC (N = 138, selected at random across the surface), AuNC-1 (N = 68), AuNC-2 (N = 35), AuNC-3 (N = 74) and AuNC-4 (N = 56) are indicated by the black, orange, red, purple and green distributions, respectively. Experimental parameters are as follows: v = 10 V s^{-1}, t_d = 260 µs, t_s = 671 s (*ca.* 0.27 s per pixel), E_a = –0.708 V, E_i = 0.142 V and E_f = –0.458 V (all *vs.* RHE). All *xy* scale bars indicate 500 nm. The data presented in **(a-d)** are not interpolated.

4. Conclusions

In conclusion, SECCM deployed in a voltammetric hopping mode regime with fine, single-channeled probes has been shown to be a robust and versatile method for the direct nanoscale topographical/electrochemical imaging of electrocatalytic materials. Spatially-resolved topographical (*z*-height) and voltammetric (*i*-*E*) data are collected synchronously to construct images (maps) which resolve active surface features on the sub-10 nm scale and create potential-resolved electrochemical activity movies comprised of hundreds of images at rates as fast as 0.25 s per pixel or 1.65 s per image frame. The experimental parameters critical to a robust scanning protocol (*e.g.*, E_a, humidity control, QRCE calibration) with high spatial resolution (*e.g.*, hopping distance) and optimal scan times (*e.g.*, *v*, approach rate, lateral movement rate) have been discussed in the context of the HER/MoS_2 system. Sub-nanoentity (*e.g.*, sub-particle) reactivity mapping has been demonstrated, with individual LSVs collected within single-crystalline {111}-oriented AuNCs (supported on GC) showing uniform (spatially-independent) activity, as expected for grain-orientation dependent electrocatalytic processes such as the HER/ORR. Although the method has been applied exclusively to reactivity mapping with electrocatalytic nanomaterials, such an approach would also be applicable to other fields of materials science (*e.g.*, corrosion science), where elucidating the correlation between nanoscale-structure (*e.g.*, crystallographic orientation) and function (*e.g.*, corrosion resistance) is a crucial step in the rational design and synthesis of functional materials.

Supplementary Information

Movies: Spatially-resolved LSV-SECCM movies obtained from the HER on the surface of bulk MoS_2 (Movie S1) and the ORR/HER on the surface of GC-supported AuNCs (Movie S2). **Figures:** SEM images of GC-supported AuNCs (Figure S1). SECCM topographical/electrochemical maps obtained on the GC support (Figure S2). *z*-height and i_{surf} line scan profile comparison, obtained from GC-supported AuNCs (Figure S3). Average LSVs obtained from GC-supported AuNCs (Figure S4).

Acknowledgements

This work was supported by a Marie Curie Individual Fellowship 702048 NEIL (C.L.B.). P.R.U. gratefully acknowledges support from a Royal Society Wolfson Research Merit Award.

References

1. J. B. Wu and H. Yang, *Acc. Chem. Res.*, 2013, **46**, 1848-1857.
2. S. E. F. Kleijn, S. C. S. Lai, M. T. M. Koper and P. R. Unwin, *Angew. Chem.-Int. Edit.*, 2014, **53**, 3558-3586.
3. P. Rodriguez and M. T. M. Koper, *Phys. Chem. Chem. Phys.*, 2014, **16**, 13583-13594.
4. P. Trogadas, V. Ramani, P. Strasser, T. F. Fuller and M. O. Coppens, *Angew. Chem.-Int. Edit.*, 2016, **55**, 122-148.
5. J. B. Sambur and P. Chen, in *Annual Review of Physical Chemistry, Vol 65*, eds. M. A. Johnson and T. J. Martinez, Annual Reviews, Palo Alto, 2014, vol. 65, pp. 395-422.
6. S. M. Oja, Y. Fan, C. M. Armstrong, P. Defnet and B. Zhang, *Anal. Chem.*, 2016, **88**, 414-430.
7. M. Kang, D. Momotenko, A. Page, D. Perry and P. R. Unwin, *Langmuir*, 2016, **32**, 7993-8008.

8. C. Kranz, *Analyst*, 2014, **139**, 336-352.

9. J. B. Sambur, T. Y. Chen, E. Choudhary, G. Q. Chen, E. J. Nissen, E. M. Thomas, N. M. Zou and P. Chen, *Nature*, 2016, **530**, 77-80.

10. A. J. Wilson and K. A. Willets, *Nano Lett.*, 2014, **14**, 939-945.

11. N. M. Andoy, X. Zhou, E. Choudhary, H. Shen, G. Liu and P. Chen, *J. Am. Chem. Soc.*, 2013, **135**, 1845-1852.

12. Y. Yu, T. Sun and M. V. Mirkin, *Anal. Chem.*, 2015, **87**, 7446-7453.

13. P. Y. Blanchard, T. Sun, Y. Yu, Z. Y. Wei, H. Matsui and M. V. Mirkin, *Langmuir*, 2016, **32**, 2500-2508.

14. J. Kim, C. Renault, N. Nioradze, N. Arroyo-Curras, K. C. Leonard and A. J. Bard, *J. Am. Chem. Soc.*, 2016, **138**, 8560-8568.

15. Y. Takahashi, A. I. Shevchuk, P. Novak, B. Babakinejad, J. Macpherson, P. R. Unwin, H. Shiku, J. Gorelik, D. Klenerman, Y. E. Korchev and T. Matsue, *Proc. Natl. Acad. Sci. U. S. A.*, 2012, **109**, 11540-11545.

16. J. V. Macpherson and P. R. Unwin, *Anal. Chem.*, 2000, **72**, 276-285.

17. C. Kranz, G. Friedbacher, B. Mizaikoff, A. Lugstein, J. Smoliner and E. Bertagnolli, *Anal. Chem.*, 2001, **73**, 2491-2500.

18. A. Page, M. Kang, A. Armitstead, D. Perry and P. R. Unwin, *Anal. Chem.*, 2017, **89**, 3021-3028.

19. M. A. O'Connell, J. R. Lewis and A. J. Wain, *Chem. Commun.*, 2015, **51**, 10314-10317.

20. D. Momotenko, K. McKelvey, M. Kang, G. N. Meloni and P. R. Unwin, *Anal. Chem.*, 2016, **88**, 2838-2846.

21. M. Kang, D. Perry, C. L. Bentley, G. West, A. Page and P. R. Unwin, *ACS Nano*, 2017, **11**, 9525-9535.

22. R. W. Murray, *Chem. Rev.*, 2008, **108**, 2688-2720.

23. L. Jacobse, S. J. Raaijman and M. T. M. Koper, *Phys. Chem. Chem. Phys.*, 2016, **18**, 28451-28457.

24. C. L. Bentley, M. Kang and P. R. Unwin, *Curr. Opin. Electrochem.*, 2017, **6**, 23-30.

25. N. Ebejer, A. G. Güell, S. C. S. Lai, K. McKelvey, M. E. Snowden and P. R. Unwin, in *Annual Review of Analytical Chemistry, Vol 6*, eds. R. G. Cooks and J. E. Pemberton, Annual Reviews, Palo Alto, 2013, vol. 6, pp. 329-351.

26. Y. Takahashi, A. Kumatani, H. Munakata, H. Inomata, K. Ito, K. Ino, H. Shiku, P. R. Unwin, Y. E. Korchev, K. Kanamura and T. Matsue, *Nat. Commun.*, 2014, **5**, 1-7.

27. A. G. Güell, A. S. Cuharuc, Y.-R. Kim, G. Zhang, S.-y. Tan, N. Ebejer and P. R. Unwin, *ACS Nano*, 2015, **9**, 3558-3571.

28. R. G. Mariano, K. McKelvey, H. S. White and M. W. Kanan, *Science*, 2017, **358**, 1187-1192.

29. C. L. Bentley, C. Andronescu, M. Smialkowski, M. Kang, T. Tarnev, B. Marler, P. R. Unwin, U. P. Apfel and W. Schuhmann, *Angew Chem Int Ed Engl*, 2018, DOI: 10.1002/anie.201712679, *in press*.

30. B. D. B. Aaronson, C. H. Chen, H. J. Li, M. T. M. Koper, S. C. S. Lai and P. R. Unwin, *J. Am. Chem. Soc.*, 2013, **135**, 3873-3880.

31. C.-H. Chen, K. E. Meadows, A. Cuharuc, S. C. S. Lai and P. R. Unwin, *Phys. Chem. Chem. Phys.*, 2014, **16**, 18545-18552.

32. C.-H. Chen, L. Jacobse, K. McKelvey, S. C. S. Lai, M. T. M. Koper and P. R. Unwin, *Anal. Chem.*, 2015, **87**, 5782-5789.

33. S. P. E, Y.-R. Kim, D. Perry, C. L. Bentley and P. R. Unwin, *ACS Appl. Mater. Interfaces*, 2016, **8**, 30458–30466.

34. C. L. Bentley, M. Kang, F. M. Maddar, F. Li, M. Walker, J. Zhang and P. R. Unwin, *Chem. Sci.*, 2017, **8**, 6583-6593.

35. P. R. Unwin, A. G. Güell and G. Zhang, *Acc. Chem. Res.*, 2016, **49**, 2041-2048.

36. J. C. Byers, A. G. Güell and P. R. Unwin, *J. Am. Chem. Soc.*, 2014, **136**, 11252-11255.

37. S. C. S. Lai, P. V. Dudin, J. V. Macpherson and P. R. Unwin, *J. Am. Chem. Soc.*, 2011, **133**, 10744-10747.

38. D. Momotenko, J. C. Byers, K. McKelvey, M. Kang and P. R. Unwin, *ACS Nano*, 2015, **9**, 8942-8952.

39. C. L. Bentley, M. Kang and P. R. Unwin, *J. Am. Chem. Soc.*, 2017, **139**, 16813-16821.

40. K. S. Novoselov, A. K. Geim, S. V. Morozov, D. Jiang, Y. Zhang, S. V. Dubonos, I. V. Grigorieva and A. A. Firsov, *Science*, 2004, **306**, 666-669.

41. S. S. Shankar, A. Rai, B. Ankamwar, A. Singh, A. Ahmad and M. Sastry, *Nat. Mater.*, 2004, **3**, 482-488.

42. G. Zhang, S.-y. Tan, A. N. Patel and P. R. Unwin, *Phys. Chem. Chem. Phys.*, 2016, **18**, 32387-32395.

43. M. E. Snowden, A. G. Güell, S. C. S. Lai, K. McKelvey, N. Ebejer, M. A. O'Connell, A. W. Colburn and P. R. Unwin, *Anal. Chem.*, 2012, **84**, 2483-2491.

44. A. Page, D. Perry and P. R. Unwin, *Proc. Royal Soc. A*, 2017, **473**.

45. A. Page, D. Perry, P. Young, D. Mitchell, B. G. Frenguelli and P. R. Unwin, *Anal. Chem.*, 2016, **88**, 10854-10859.

46. C. G. Williams, M. A. Edwards, A. L. Colley, J. V. Macpherson and P. R. Unwin, *Anal. Chem.*, 2009, **81**, 2486-2495.

47. J. D. Benck, T. R. Hellstern, J. Kibsgaard, P. Chakthranont and T. F. Jaramillo, *ACS Catal.*, 2014, **4**, 3957-3971.

48. Z. W. Seh, J. Kibsgaard, C. F. Dickens, I. Chorkendorff, J. K. Nørskov and T. F. Jaramillo, *Science*, 2017, **355**, 146.

49. Q. Li, S. B. Xie, Z. W. Liang, X. Meng, S. J. Liu, H. H. Girault and Y. H. Shao, *Angew. Chem.-Int. Edit.*, 2009, **48**, 8010-8013.

50. P. Novak, A. Shevchuk, P. Ruenraroengsak, M. Miragoli, A. J. Thorley, D. Klenerman, M. J. Lab, T. D. Tetley, J. Gorelik and Y. E. Korchev, *Nano Lett.*, 2014, **14**, 1202-1207.

51. N. Ebejer, M. Schnippering, A. W. Colburn, M. A. Edwards and P. R. Unwin, *Anal. Chem.*, 2010, **82**, 9141-9145.

52. M. T. M. Koper, *Nanoscale*, 2011, **3**, 2054-2073.

53. M.-C. Daniel and D. Astruc, *Chem. Rev.*, 2004, **104**, 293-346.

54. Y. Shao, Y. Jin and S. Dong, *Chem. Commun.*, 2004, DOI: 10.1039/B315732F, 1104-1105.

55. M. Grzelczak, J. Perez-Juste, P. Mulvaney and L. M. Liz-Marzan, *Chem. Soc. Rev.*, 2008, **37**, 1783-1791.